Journal of Nuclear Materials 397 (2010) 109–115

Contents lists available at ScienceDirect

Journal of Nuclear Materials

journal homepage: www.elsevier.com/locate/jnucmat

Residual strain measurement and grain boundary characterization in the heat-affected zone of a weld joint between Alloy 690TT and Alloy 52

J. Hou [a,b], T. Shoji [a], Z.P. Lu [a], Q.J. Peng [a,*], J.Q. Wang [b], E.-H. Han [b], W. Ke [b]

[a] Fracture and Reliability Research Institute, Graduate School of Engineering, Tohoku University. 6-6-01, Aramaki Aoba, Aoba-ku, Sendai 980-8579, Japan
[b] State Key Laboratory for Corrosion and Protection, Institute of Metal Research, Chinese Academy of Sciences, 62 Wencui Road, Shenyang 110016, China

ARTICLE INFO

Article history:
Received 18 September 2009
Accepted 25 December 2009

ABSTRACT

The distributions of residual strains and grain boundary microstructures were investigated in the heat-affected zone (HAZ) of a weld joint between Alloy 690TT (thermally treated) and Alloy 52 using electron backscatter diffraction (EBSD) and transmission electron microscopy. The distributions of residual strains were examined at the top, middle, and root of the HAZ using EBSD to obtain the grain average misorientation. The weld residual strain increased from the top of the weld to the root while the peak of strain approached the fusion boundary (FB) in the HAZ. The maximum strains and their distances to the FB in the top, middle, and root was 15% and 800 μm, 17% and 600 μm, 20% and 200 μm, respectively. The fraction of Σ3 special boundaries was about 40% in the HAZ but with obvious deviations from the structure of ideal boundaries. The HAZ region is considered to sustain the highest susceptibility to SCC at the root of the weld.

1. Introduction

The purpose of the work in this paper is to characterize the weld heat-affected zone (HAZ) between Alloy 690TT and Alloy 52. These characterizations include mainly the local residual strains and local structures of grains. This work is important since such welds are now being used to replace previous welds with Alloy 600 and associated welding materials. Plant experiences and laboratory experiments have shown that Alloy 600 and its associated weld metals are susceptible to stress corrosion cracking (SCC) in the environments of water reactors [1–6]. It has been reported that the growth rates of SCC in Alloy 600 HAZ in simulated pressurized water reactor primary water is significantly higher than those in the base metal [7–9].

As a result of the extensive SCC of Alloy 600 and its weld metals, Alloy 690 and its compatible weld metals, Alloys 52 and 152, which contain higher concentrations of Cr, are now being used as repairs or replacement components owing to their resistance to SCC. Alloy 690 and its weld metals have been free from cracking in the primary loop of reactors for over 15 years of operation. However, there are still concerns about SCC of welded Alloy 690 after longer times [10].

Welds are especially prone to SCC owing to high local stresses, which are produced by shrinkage, and to local cold work [11–14]. The maximum residual stresses, which are produced in welding, are usually higher than the yield strength of material, so that SCC can be produced without applied stresses [13]. Weld shrinkage immediately adjacent to the fusion boundary (FB) produces a large and consistent source of cold work up to 20–30%, which can accelerate the crack growth rate of SCC by a factor of about 10 in Alloy 690 [11,12]. The hardened zone of the HAZ has a width of about 2 mm in an Alloy 690 HAZ [9].

Grain boundary microstructure is important to the intergranular cracking which is the main mode of SCC of austenitic alloys in high temperature water. Investigations of SCC in Ni-base alloys have revealed generally that there has been no intergranular SCC (IGSCC) at Σ3 boundaries, and only Σ3 boundaries were suggested as the real special boundary [15–17]. However, in Ni-base alloys and stainless steels, SCC have been observed at the Σ3 boundaries where there are large deviation degrees from ideal grain boundary structure [17,18]. Therefore, investigating the grain boundary characters and degrees of deviation from ideal special boundary structure is important for clarifying possible effects of susceptible microstructures at grain boundaries on IGSCC.

In this study, distributions of residual strains and microstructures of grain boundaries were investigated quantitatively in the HAZ of a weld joint between Alloy 690TT and Alloy 52. The mechanical and metallographic properties were also investigated.

2. Experimental

The base metal, Alloy 690, was heat treated at 1075 °C for 1 h, air cooled, and thermally treated (TT) at 700 °C for 15 h. A weld joint was then fabricated by filling Alloy 52 to a J-groove in a plate of Alloy 690TT by multi-pass argon arc welding (current: 120–235

* Corresponding author. Tel.: +81 22 795 7520; fax: +81 22 795 7543.
E-mail address: qpeng@rift.mech.tohoku.ac.jp (Q.J. Peng).

0022-3115/$ - see front matter © 2009 Elsevier B.V. All rights reserved.
doi:10.1016/j.jnucmat.2009.12.016

A, voltage: 12–13 V, interpass temperature: <149 °C, speed: 10 cm/min, heat input: 17.9 kJ/cm, 33 passes). Geometry and dimension of the weld joint are schematically shown in Fig. 1a. Chemical compositions of both metals are given in Table 1.

Metallographic microstructure of the weld joint was characterized with a Hitachi 4300 scanning electron microscope (SEM). The SEM is equipped with a camera that was used for analyzing the microstructures of grain boundaries and distributions of residual strains in the HAZ region by electron backscatter diffraction (EBSD) in connection with the TSL software.

The qualitative strains were estimated by measuring the amount of intra-grain average misorientation (GAM) [19], which was calculated by indexing and averaging the misorientations of neighbor-to-neighbor points within the grains. The samples, which were used for EBSD examination, were strips which were cut from the regions across the FB. The specimens, A, B, and C, were extracted from the top, middle and root locations of the weld joint as shown in Fig. 1b. Areas about 1.4 mm × 7 mm across the FB from weld metal to HAZ were examined by EBSD on the surfaces of each specimen. This area is sufficiently large to obtain reliable results. The GAM data were calculated and averaged in 200 μm segments (grains located within ±100 μm from the FB were assigned to the 0 μm location (FB segment), 100–300 μm = 200 μm and 300–500 μm = 400 μm in HAZ, and so on). The step size for EBSD scanning was set as 2 μm using the voltage of 25 kV.

For the observation of the grain boundary precipitates, a slice was taken in the HAZ from specimen C at the root of the weld joint. It was then punched into pieces of 3 mm diameter with the center distances of 1, 3 and 6 mm to the FB, as schematically shown in Fig. 1c. Following thinning by ion milling, the pieces were examined by a Hitachi HF-2000 transmission electron microscopy (TEM) to identify the grain boundary precipitates.

For quantitatively estimating the residual strain in the weld joint, tensile specimens of as-received Alloy 690TT were machined for calibrating the dependence of GAM on tensile strain. The tension samples have a gauge part of 4 mm × 7 mm and with a thickness of 2 mm, which was schematically shown in Fig. 1d. One tensile specimen was strained to 5%, 10%, 15%, 20% and 25%, consecutively. The strains were controlled by a BE120-05AA type electric resistance strain gauge, which was glued to one surface of the gauge section in the EBSD scanning region. EBSD scanning was performed on one location of these strained specimens step by step under the same condition of examination with the specimens A, B and C.

Due to the similar microstructure of HAZ to that of the base metal, the relationship between GAM and tensile strain is applicable to the estimation of residual strain in HAZ. Also since the GAM measurement depends on the change of intra-grain orientation generated by either tensile or compressive plastic deformation, the relationship is applicable to the estimation of the compressive residual strain in the weld joint as well. With regard to the estimation of the residual strain in the weld metal, it is likely errors may be generated when using the relationship that was obtained from the base metal due to the difference in the morphology and size of the grain of base and weld metals. Nevertheless, the errors are expected not to be much since the GAM was obtained from a large area on the specimen (1.4 mm × 0.2 mm) that the variations of the strain with grains were averaged. In addition, the focus of the current study is on the residual strain in HAZ that may have high susceptibility to SCC in the weld joint as to be discussed later.

Micro-hardness was measured in the FB regions from Alloy 52 to the HAZ side using a SHIMADZU HMV micro-hardness tester with a load of 0.9807 N and a holding time of 20 s.

3. Results and discussion

Large dendritic grains approximately perpendicular to the FB were observed by SEM in the dilution zone of the Alloy 52 side as shown in Fig. 2. The grains in the HAZ side were smaller and contained some twin boundaries. The inserts of higher magnification in Fig. 2 indicated high coverage of grain boundaries by carbide precipitates. The carbides are semi-continuous and decreased in size from the top to the bottom of the weld as shown successively in Fig. 2a, b and c. Relatively large square TiN inclusions were dispersed on the HAZ side in both intragranular and transgranular locations.

The carbide precipitates in the grain boundaries and the TiN inclusions were examined with the TEM. In the specimen which is shown in Fig. 3a with a distance of 1 mm from the FB, a small, about 1 μm, and elongated TiN inclusion was observed and confirmed by its diffraction pattern and EDX-spot composition analysis, either inside the grain or crossing the grain boundaries along

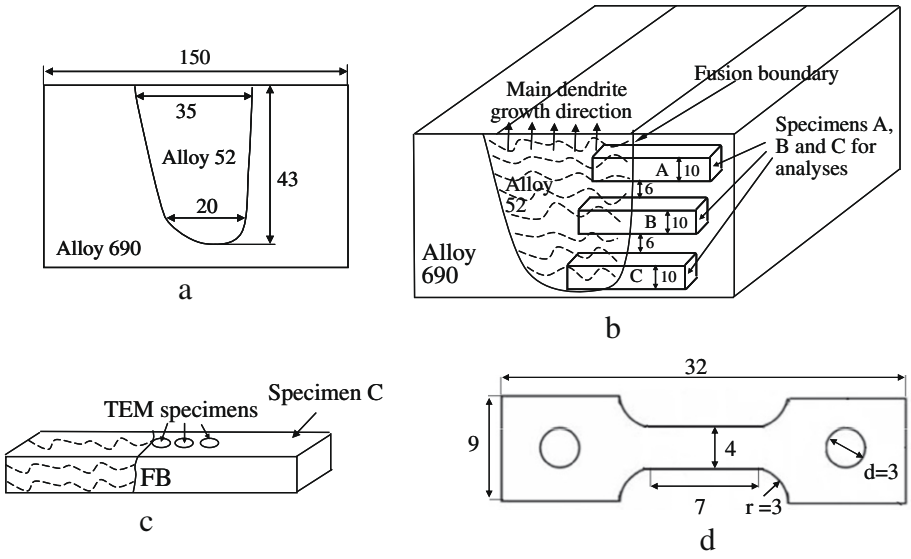

Fig. 1. Schematic drawings showing the dimensions of the weld joint between Alloy 690 and Alloy 52 (a), the specimen extraction from the weld joint (b), TEM specimens taken from specimen C (c), and the geometry and size of the tensile specimens machined using as-received Alloy 690TT for calibrating the dependence of intragranular average misorientation (GAM) on tensile strain (d).

Table 1
Chemical compositions of base metal and weld metal (wt.%).

	Fe	C	Si	Mn	Ni	S	Cr	P	Cu
Alloy 690TT	10.13	0.02	0.11	0.16	59.42	0.001	29.53	0.006	0.01
Alloy 52	10.23	0.025	0.15	0.24	59.10	0.001	28.98	0.003	0.01

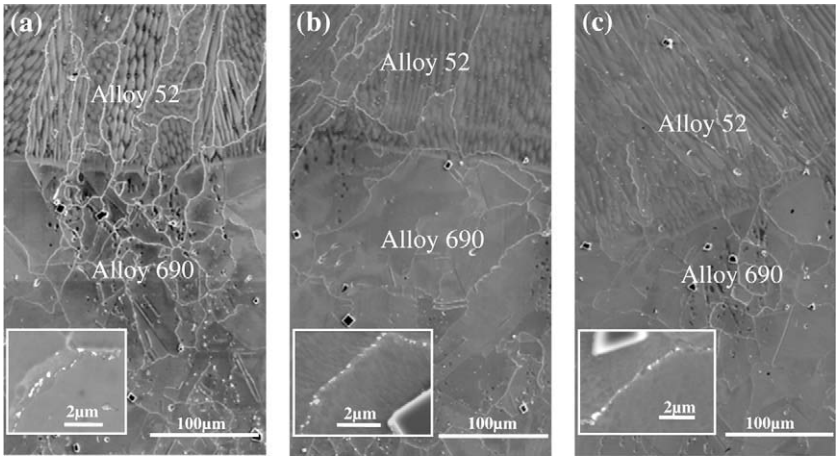

Fig. 2. Metallographic observation of weld top, specimen A (a) weld middle, specimen B (b) and weld root, specimen C (c).

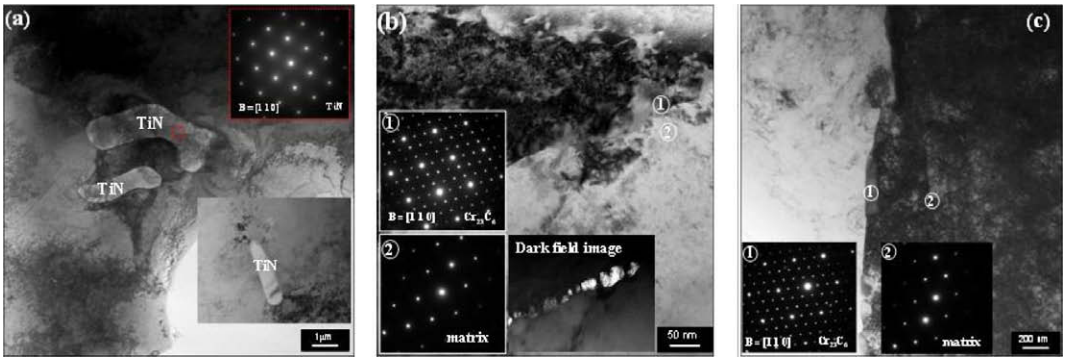

Fig. 3. TEM pictures showing intragranular TiN inclusions (a), carbide precipitations on grain boundary in HAZ with the distance from fusion boundary of 1 mm (b), and carbide precipitations on grain boundary in HAZ with the distance from the fusion boundary of 6 mm (c).

the axial direction. The carbides on grain boundaries were confirmed to be $Cr_{23}C_6$ by diffraction from EDX-spot analysis, Fig. 3b. The inserted dark field image in Fig. 3b shows that carbide precipitates are almost continuous on the grain boundary. The inserted diffraction patterns in this figure indicate that carbides are coherent with one of the neighboring grains.

In the specimen with a distance of 6 mm from the FB, the elongated grain boundary carbides are larger with decreased boundary coverage, while they are still coherent with one of the neighboring grains as shown in Fig. 3c. The larger TiN in this specimen is square but is not shown here. The higher residual strains and repeated heat cycles in the HAZ immediately near the FB may have produced the higher density of carbides.

The hardness in the HAZ was measured along three lines across the FB in each of the three specimens as shown in Fig. 4a. Bands of scattered data points of hardness across the HAZ were obtained, which is due mainly to the less accurate measurements with relatively large sizes of indentations (around 25 μm) and the high-density of carbide precipitates and TiN inclusions. The obviously hardened area in the HAZ was within about 2 mm from the FB, where the average hardness was about 240 HV, which is generally consistent with the previous results reported by Shoji et al. [9]. In the tensile specimens under consecutive strains, the measured hardness was approximately linear with the strains as shown in Fig. 4b. A hardness of 240 HV was approximately consistent with that of a 15% strained specimen.

Maps of intragranular average misorientation and the grain boundary characters across the FB in specimens A, B, and C are shown in Fig. 5a, b and c, respectively. In these maps, the black boundaries represent the random high-angle boundaries, the red represent the Σ3 special boundaries, and the white represent the low-angle boundaries ($5 < \theta < 15°$). The GAM was used to estimate the residual strains by the rainbow color code, in which the blue color denotes the minimum and the red color denotes the maximum intragranular misorientation, as shown in Fig. 5. The grains in the HAZ side with higher GAM were smaller and grew epitaxially from the FB. The grain boundaries in the weld metal side were almost all random boundaries while in the HAZ side a high fraction of Σ3 special boundaries (denoted as the red lines) was observed.

The calculated GAM as a function of distance from the FB in specimens A, B and C is shown in Fig. 6. The GAM for tensile specimens strained to 0%, 5%, 10%, 15%, 20% and 25% by tension was

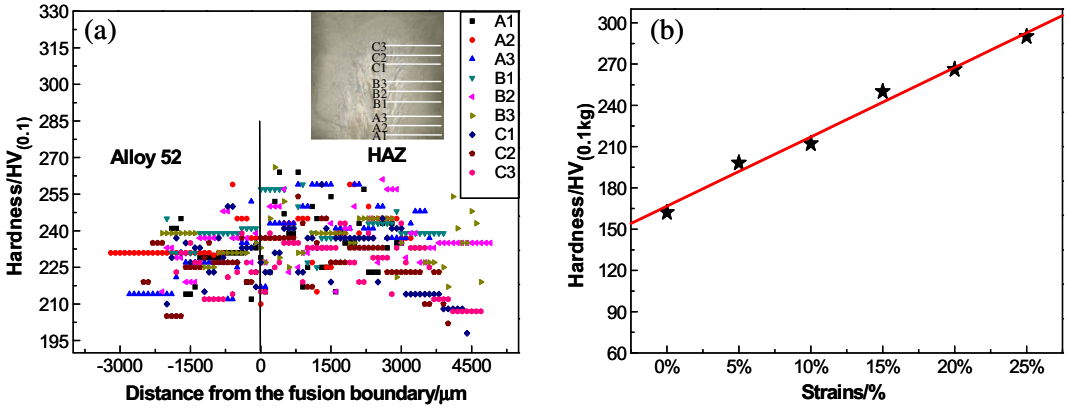

Fig. 4. The distribution of Vickers hardness of (a) across the fusion boundary from Alloy 52 to Alloy 690 HAZ and (b) the series tensile specimens of Alloy 690 base metal.

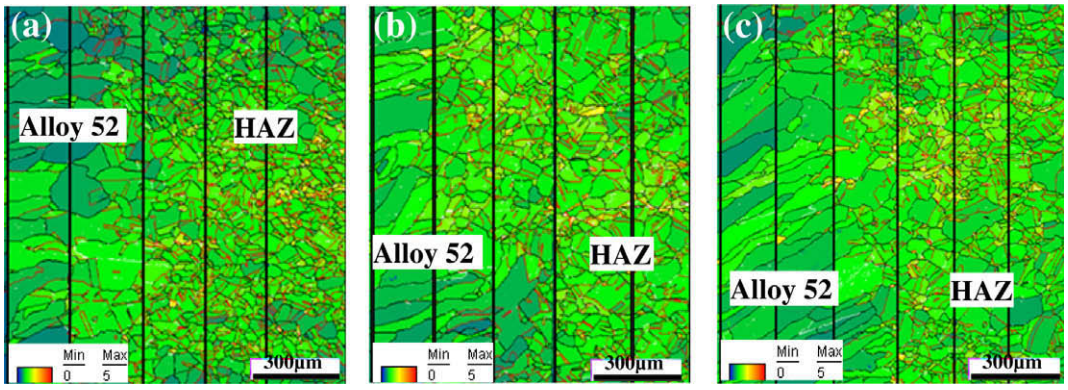

Fig. 5. GAM and grain boundary character maps in the regions across the fusion boundary from Alloy 52 to Alloy 690 HAZ of specimen A (a), specimen B (b) and specimen C (c). In the maps, black lines denote the random high-angle boundaries, red lines denote the Σ3 special boundaries, and white lines denote the low-angle boundary ($5° < \theta < 15°$). (For interpretation of the references to colour in this figure legend, the reader is referred to the web version of this article.)

also calculated as a function of tensile strains as shown in Fig. 6. The relationship between the GAM and the tensile strains is linear with a high correlation coefficient ($R^2 = 0.997$). Combining the GAM of specimens A, B, C with that of tensile specimens produced the quantified strain distribution in the regions across the FB from the weld metal to HAZ as shown in Fig. 7. The quantitative strain distributions obtained by EBSD provided more accurate and detailed information for the hardened regions in the HAZ than the hardness measurement. The peak magnitudes of strains were immediately near the FB, within a distance depending on the location in the weld joint, and then decreased significantly. In specimen A, which was extracted from the top of the weld joint, the highest strain was about 15%, with a distance of around 800 μm from the FB. In specimen B, which was extracted from the middle of the weld joint, the peak magnitude of strain was about 17% at a distance of 600 μm from the FB, while the peak width was narrower. Specimen C, which was extracted from the root of the weld joint, exhibited the highest peak magnitude of about 20% at a distance of about 200 μm from the FB with the narrowest peak width. The strains imposed on the HAZ side were generated by the heating, high temperature and welding shrinkage during the welding process. The magnitudes of peak strains increased from the top to root along the fusion line while the locations of peak strains were closer to the FB but were not on the FB. Further, residual strains were highest at the weld root. The weld residual strains may intensify SCC similar to effects of cold work.

The distribution of residual strains described above may have been produced by the thermal histories of the welds that vary with locations. The conventional arc welding processes generate a large amount of heat within the HAZ. The thermal cycles produced the highest peak temperature and a more rapid temperature rise and cooling rate nearer to the FB, which decreased as the distance from the FB increased [20]. This caused a peak of the strain close to the FB and a gradual decrease of strain away from the FB in the HAZ. Also the maximum repeated thermal cycles at the root of the weld produced the highest magnitude of residual strains. The reason that the location of peak residual strains became nearer to the FB from weld top to weld root is currently unclear, while it is likely due to the changes in thermal history and the distribution of heat. One difficulty in clarifying the reason is that the distribution of heat during the welding process is highly non-uniform and relevant to many variations such as the geometry and size of the weld pool, the material property, and the multipass welding [21–23]. Further mechanistic study is required to understand the relationship between the history and distribution of the heat and the distribution of residual strain.

The grain boundary character distribution (GBCD) and the degrees of deviation from the ideal Σ3 boundary misorientation for the Σ3 boundaries of the HAZ in specimens A, B and C were calculated using the maps shown in Fig. 5. The calculation results were compared to that of tensile specimens as shown in Fig. 8. The grain boundaries in this study were classified into three types: low-angle

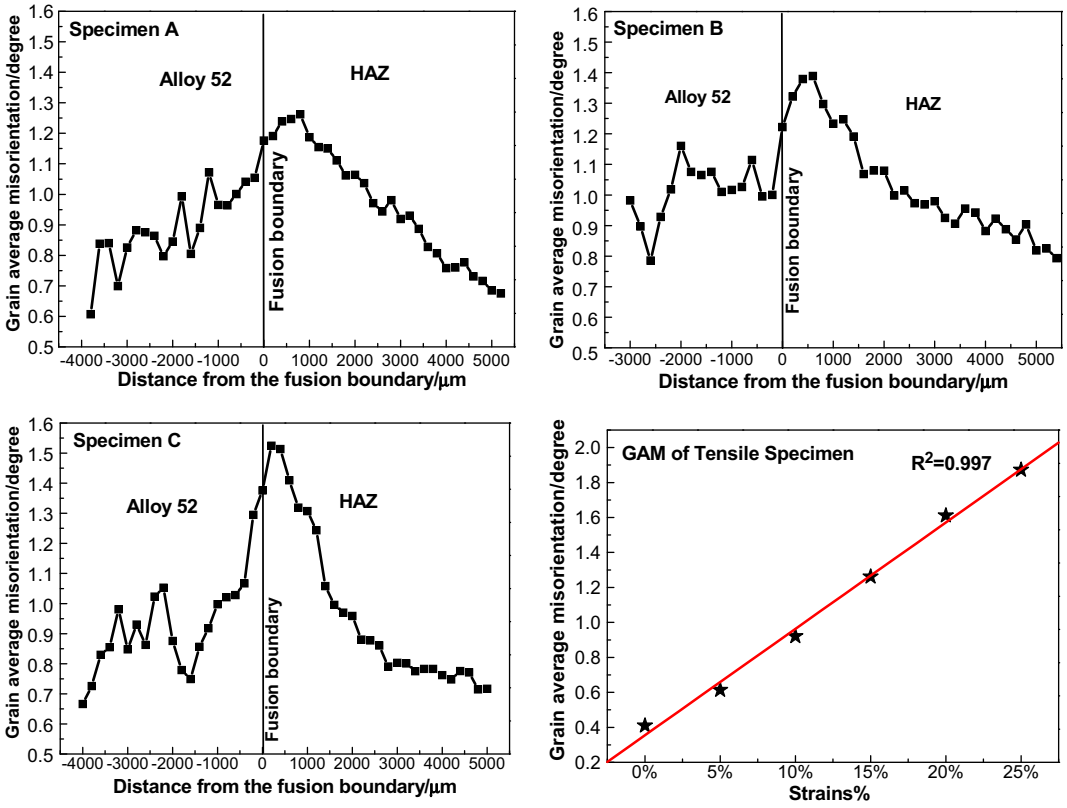

Fig. 6. The GAM distribution in specimens A, B, and C and calibrated series of tensile specimens (strained 5%, 10%, 15%, 20% and 25% in tension at room temperature).

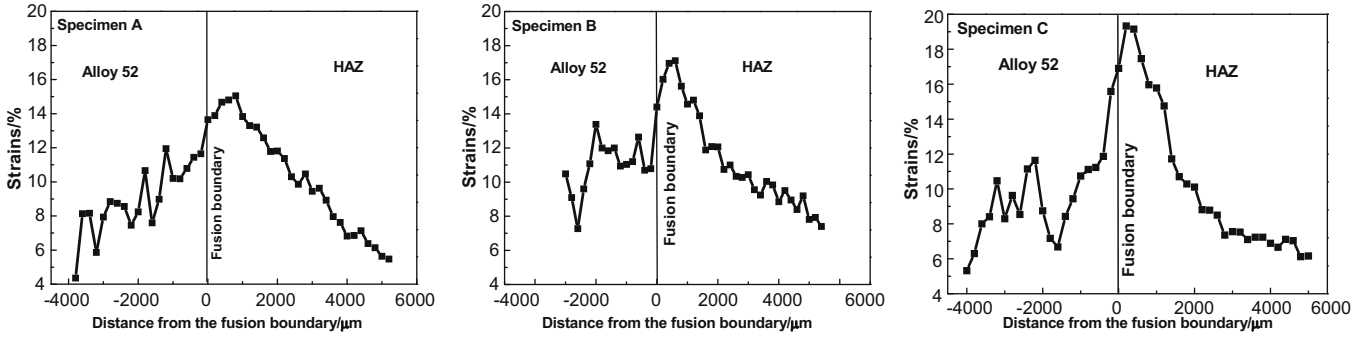

Fig. 7. Strain distribution through the fusion boundary zone from Alloy 52 to Alloy 690 HAZ of specimens A, B and C, calculated by comparing the GAM with that of series tensile specimens.

boundary (LAB), special Σ3 boundary, and random grain boundary (RGB). The maximum angular deviation $\Delta\theta$ from the ideal coincidence site lattice (CSL) misorientation for which the boundary still maintains its CSL structure can be estimated from the acceptance criterion introduced by Palumbo–Aust criterion ($\Delta\theta_m = 15* \Sigma^{-5/6}$) [24]. As can be seen in Fig. 8a and b, the fractions of Σ3 special boundaries in the HAZ of specimens A, B, C were about 40%, which is much less than the 65% of the base Alloy 690TT. Further, the fraction of Σ3 special boundaries decreased significantly with increasing tensile strains, while the low angle and random boundary increased with increasing the strains. This phenomenon was related to the grain boundary transition, increased generation of dislocations and the arrangements of dislocations in front of the boundaries [25]. The fraction of Σ3 boundaries in HAZ was similar to that of the tensile specimen with a tensile strain of about 10%. The HAZ region deviates significantly from the ideal misorientation from the top to root with respect to the ideal Σ3 misorientation as shown in Fig. 8c. In the tensile specimens, the degrees of deviation increased with increasing strains as shown in Fig. 8d. The deviation from the Σ3 structure in the HAZ can potentially reduce the resistance of HAZ to SCC by decreasing the SCC resistance of Σ3 special boundaries.

Comparing the HAZ with the 25% strained specimen, it was obvious that the welding process in the HAZ generated higher deviation from the ideal Σ3 boundary than the 25% deformation. However, as can be seen in Fig. 4, the hardness of HAZ is approximately equal to that of the 15% strained specimen, indicating the inconsistence between the hardness and deformation level of the Σ3 boundary. This is likely caused by the strain concentration adjacent to the Σ3 boundary. The effectiveness of Σ3 boundaries as barriers to plastic flow has been identified [26], which results in deformation accumulation at the boundary during the process of

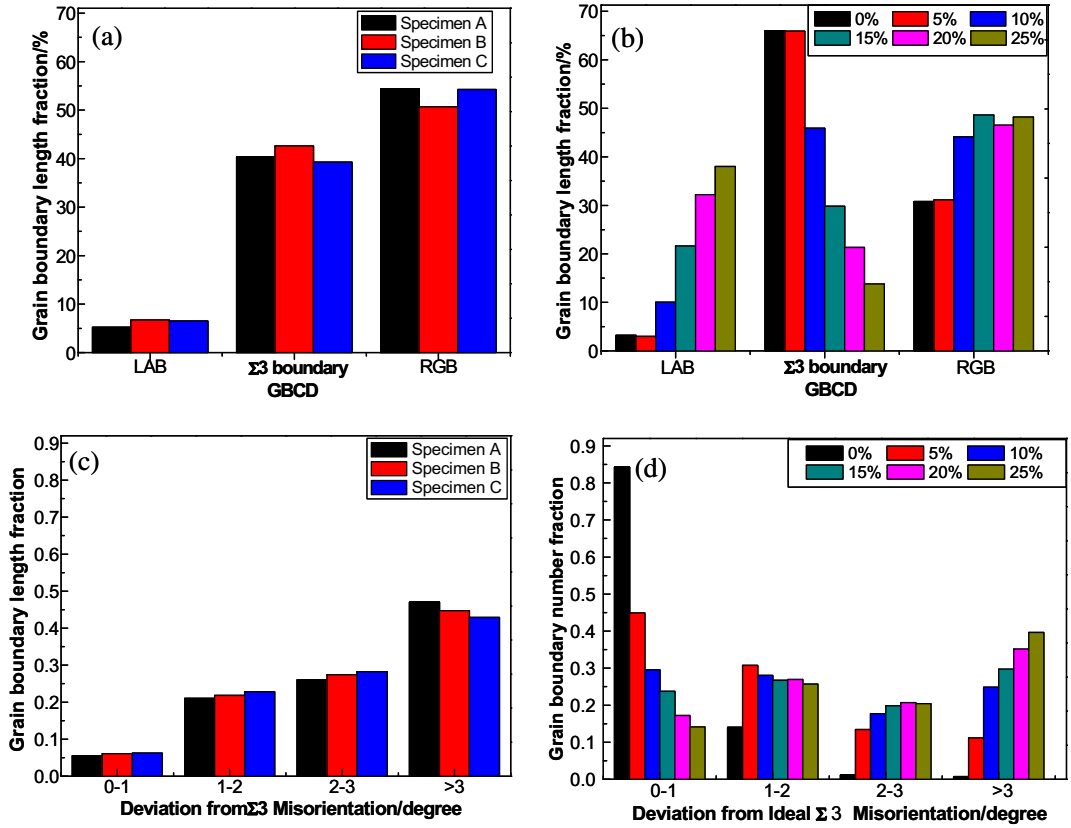

Fig. 8. Grain boundary character distribution (GBCD) of the HAZ in specimens A, B, C (a) and series tensile specimens (b), the deviation degrees from the ideal Σ3 misorientation of the HAZ (c) and series tensile specimens (d).

straining. Since the average deformation in the grain contributes more to the hardness, the higher deformation at the Σ3 boundary may have not caused higher hardness of the alloy.

The distribution of residual strains and the character of grain boundaries, which are discussed here, enable better understanding of the possible SCC behavior of the HAZ. The welding process degraded the microstructure in the HAZ severely by decreasing the fraction of Σ3 boundaries and increasing degrees of deviation from ideal Σ3 special boundary structure, which suggests a high susceptibility of the HAZ to SCC, although the microstructural deterioration was nearly independent of locations in welding deposits. Combining the effects of weld residual strains and microstructural deterioration, the highest residual strain near the FB at the weld root implies that the HAZ region could sustain the highest susceptibility to SCC at the root of the weld.

4. Conclusions

The metallographic microstructure, mechanical properties, residual strain distribution and grain boundary characteristics in the HAZ of a weld joint between Alloy 690TT and Alloy 52 were studied. The quantitative measurement of residual strains in the HAZ was performed using a calibrated tensile specimen fabricated from as-received Alloy 690TT. From this work the followings are concluded:

1. The dendritic grains in Alloy 52 were epitaxial with the base metal with perpendicular orientation to the FB. The grains on the HAZ side were smaller with higher coverage of carbide precipitates at the grain boundaries. The grains also contained intragranularly dispersed TiN inclusions.
2. The HAZ was hardened to about 240 HV within a distance of approximately 2 mm away from the FB.
3. The weld residual strains increased from weld top to weld root while the strain peak became closer to the FB in the HAZ. The maximum strains and their distances to the FB in top, middle, and root were 15% and 800 μm, 17% and 600 μm, and 20%, and 200 μm, respectively.
4. The fraction of Σ3 boundaries was about 40% in the HAZ, which is close to that in the 10% tensile strained specimen. The degrees of deviation from the ideal Σ3 structure in HAZ were more significant than that in the 25% tensile strained specimen, indicating that the welding process deteriorated the grain boundary microstructures.
5. Based on both the residual strain distributions and the grain boundary deteriorations, the highest susceptibility to SCC in the HAZ region may occur in the weld root near the fusion boundary.

Acknowledgements

This research was supported by programs of the Grant-in Aid for Scientific Research (S) 17106002 and (C) 20560063, Japan Society for the Promotion of Science. The authors (J. Hou, J.Q. Wang, E-H. Han and W. Ke) would thank the Special Funds for the Major State Basic Research Projects G2006CB605000 in China. Authors are also thankful to Prof. R.W. Staehle and Prof. T. Yonezawa for their invaluable discussions and suggestions.

References

[1] P.M. Scott, P. Combrade, On the mechanism of stress corrosion crack initiation and growth in alloy 600 exposed to PWR primary water, in: 11th International

Symposium on Environmental Degradation of Materials in Nuclear Power Systems – Water Reactors, Skamania, ANS, 2003.
[2] S.L. Hong, J.M. Boursier, C. Amzallag, J. Daret, Measurement of stress corrosion growth rates in weld alloy 182 in primary water, in: The 10th International Symposium on Environmental Degradation of Materials in Nuclear Power Systems – Water Reactors, NACE, 2001.
[3] W.H. Bamford, J. Foster, K.R. Hsu, L. Tunon-Sanjur, A. McIlree, Alloy 182 weld crack growth, and its impact on service-induced cracking in operating PWR plant piping, in: The 10th International Symposium on Environmental Degradation of Materials in Nuclear Power Systems – Water Reactors, NACE, 2001.
[4] C. Amzallag, J.M. Boursier, C. Pages, C. Gimond, Stress corrosion life assessment of 182 and 82 welds used in PWR components, in: the 10th International Symposium on Environmental Degradation of Materials in Nuclear Power Systems – Water Reactors, NACE, 2001.
[5] Q.J. Peng, T. Shoji, Key Eng. Mater. 261–263 (2004) 943–948.
[6] Q.J. Peng, T. Shoji, H. Yamauchi, Y. Takeda, Corros. Sci. 49 (2007) 2767–2780.
[7] S. Yamazaki, Z. Lu, Y. Ito, Y. Takeda, T. Shoji, Corros. Sci. 50 (2008) 835–846.
[8] G.A. Young, N. Lewis, D.S. Morton, The stress corrosion crack growth rate of alloy 600 Heat affected zones exposed to high purity water, in: Prof. Conference on Vessel Head Penetration Inspection, Cracking and Repairs, USNRC, 2003, pp. 309–324.
[9] T. Shoji, Z.P. Lu, S. Yamazaki, The effect of strain-hardening on PWSCC of nickel-base alloys 600 and alloy 690, in: Proc. 14th International Conference Environmental Degradation of Materials in Nuclear Power Systems, Virginia Beach, Virginia. USA, ANS, August 23–27, 2009.
[10] R.A. Page, A. McMinn, Stress corrosion cracking resistance of alloys 600 and 690 and compatible weld metals in BWRs, in: EPRI Report NP-5882M, Palo Alto, CA, 1988, p. 1.
[11] P. Andresen, Alloy 690 base metal product forms, in: NRC/EPRI Meeting, 2008.
[12] P. Andresen, Crack initiation studies in alloy 690 & weld metals, in: NRC/EPRI Meeting, 2008.
[13] B.T. Lu, Z.K. Chen, J.L. Luo, B.M. Patchett, Z.H. Xu, Electrochim. Acta 50 (2005) 1391–1403.
[14] H. Xue, K. Ogawa, T. Shoji, Nucl. Eng. Des. 239 (2009) 628–640.
[15] D.C. Crawford, G.S. Was, Metall. Trans. A 23 (1992) 1195–1206.
[16] V.Y. Gertsman, K. Tangri, R.Z. Valiev, Acta Metall. Mater. (1994) 1785–1804.
[17] Y. Pan, B.L. Adams, T. Olson, N. Panayotou, Acta Mater. 44 (1996) 4685–4695.
[18] V.Y. Gertsman, S.M. Bruemmer, Acta Mater. 49 (2001) 1589–1598.
[19] T.M. Angeliu, P.L. Andresen, E. Hall, J.A. Sutliff, S. Sitzman, R.M. Horn, in: Ninth International Symposium on Environmental Degradation of Materials in Nuclear Power Systems-Water Reactors, TMS, Warrendale, PA 15086-7528, 1999.
[20] H.T. Lee, J.L. Wu, Corros. Sci. 51 (2009) 733–743.
[21] D. Gery, H. Long, P. Maropoulos, J. Mater. Process Technol. 167 (2005) 393–401.
[22] S. Murugan, P.V. Kumar, B. Raj, M.S.C. Bose, Int. J. Pres. Ves. Pip. 75 (1998) 891–905.
[23] M.A. Wahab, M.J. Painter, M.H. Davies, J. Mater. Process Technol. 77 (1998) 233–239.
[24] G. Palumbo, K.T. Aust, E.M. Lehockey, U. Erb, P. Lin, Scripta Mater. 38 (1998) 1685–1690.
[25] J. Hou, J.Q. Wang, W. Ke, E.H. Han, Mater. Sci. Eng.: A 518 (2009) 19–26.
[26] V. Randle, M. Coleman, Acta Mater. 57 (2009) 3410–3421.